metals

MDPI

Article

The Study of Hardness Evolution during the Tempering Process of 38MnB5Nb Ultra-High-Strength Hot Stamping Steel: Experimental Analysis and Constitutive Models

Ping Luo [1,*], Xianjun Li [1], Wenliang Zhang [1], Zhunli Tan [2,*], Minghao Zhang [1,3], Kaize Wang [1], Pengdi Hou [1], Junjie Liu [1] and Xiao Liang [4]

[1] Beijing Research Institute of Mechanical and Electrical Technology Ltd., Beijing 100083, China; imlixj@163.com (X.L.); zhangwlwork@163.com (W.Z.); d202210317@xs.ustb.edu.cn (M.Z.); wangkaize9653@163.com (K.W.); houpd1999@163.com (P.H.); 13810898783@yeah.net (J.L.)
[2] Material Science & Engineering Research Center, School of Mechanical, Electronic and Control Engineering, Beijing Jiaotong University, Beijing 100044, China
[3] School of Mechanical Engineering, University of Science and Technology Beijing, Beijing 100083, China
[4] The College of Mechanical and Electrical Engineering, Nanjing University of Aeronautics and Astronautics, Nanjing 210016, China; liangxiao@nuaa.edu.cn
* Correspondence: 18811795072@163.com (P.L.); tzli@bjtu.edu.cn (Z.T.)

Abstract: To elucidate the hardness evolution behaviors for 38MnB5Nb ultra-high-strength hot stamping steel, a series of tempering processes with varying tempering temperatures and times were carried out with a dilatometer. Meanwhile, the hardness of each sample was measured after dilatometer experiments. The results indicated that the tempering process parameters (including the tempering temperature and time) play an important role in the hardness of the studied steel. The hardness of 38MnB5Nb ultra-high-strength hot stamping steel at the quenched state is about 580 Hv, while it is 240 Hv for the quasi-annealed state. As the tempering time extends, the hardness is decreased sharply at the initial stage; then, the hardness is decreased in a quasi-linear trend with a slight slope; finally, the hardness almost keeps a constant value, which depends on the tempering temperature. In addition, the tempering process has a big effect on the mechanical properties of 38MnB5Nb ultra-high-strength hot stamping steel by increasing the product of the strength and elongation by about 40%.

Keywords: 38MnB5Nb ultra-high-strength hot stamping steel; hardness evolution; tempering; tempering ratio; modeling

check for updates

Citation: Luo, P.; Li, X.; Zhang, W.; Tan, Z.; Zhang, M.; Wang, K.; Hou, P.; Liu, J.; Liang, X. The Study of Hardness Evolution during the Tempering Process of 38MnB5Nb Ultra-High-Strength Hot Stamping Steel: Experimental Analysis and Constitutive Models. *Metals* **2023**, *13*, 1642. https://doi.org/10.3390/met13101642

Academic Editor: Saeed Sadeghpour

Received: 21 August 2023
Revised: 18 September 2023
Accepted: 21 September 2023
Published: 25 September 2023

Copyright: © 2023 by the authors. Licensee MDPI, Basel, Switzerland. This article is an open access article distributed under the terms and conditions of the Creative Commons Attribution (CC BY) license (https://creativecommons.org/licenses/by/4.0/).

1. Introduction

Because the problems of energy consumption and environmental pollution are still severe and the weight of the vehicles has a big effect on the fuel consumption, the reduction in the weight of vehicles is one of the research highlights [1–4]. According to the public data revealed by the New European Driving Cycle, fuel consumption by about 0.35 L 100 km^{-1} and CO_2 emissions by about 8.4 g km^{-1} are reduced with a weight reduction of 100 kg in a vehicle [5]. So, many efforts are made to make automobiles lightweight [6–8]. During the past few decades, vehicle components, including A-pillars, B-pillars, roof rails, and so on, have been made with ultra-high-strength steels as an ideal material [9–12]. In this context, ultra-high-strength hot stamping steels have been investigated and used to make vehicle parts [13–15].

The widely used ultra-high-strength hot stamping steel is 22MnB5 steel, and it has been utilized to manufacture vehicle components successfully, such as A-pillars, B-pillars, and so on [16–18]. The strength of the parts can be as large as 1500 MPa with the treatment of hot stamping; as a result, the thickness of them is reduced, which is beneficial for reducing the weight of vehicles. The relationships between the microalloying elements and the hydrogen

behaviors of permeation and damage for 22MnB5 hot stamping steel were investigated by Tingzhi Si et al. [5]. Their research pointed out that the addition of microalloying elements with Nb, Ti, and V is good for the resistance of hydrogen diffusion, which is beneficial for vehicle parts made of ultra-high-strength hot stamping steels. Furthermore, an interesting model that can be used to illustrate the strategies to delay the diffusion of hydrogen and to avoid the damage of hydrogen embrittlement in the 22MnB5 ultra-high-strength hot stamping steel was proposed. However, with the increase in strength, the ability to absorb crash energy is decreased, which is harmful to the drivers. To resolve the above issues, a novel hot stamping method was developed, which made it successful to manufacture a part with the material of 22MnB5 ultra-high-strength hot stamping steel consisting of both a soft region to absorb energy and a hard region to resist intrusion through a relatively simple process [19–21]. Generally, compared with the hard region, the strength is lower and the elongation is higher for the soft region. For example, in the hard regions, the tensile strength and total elongation are 1565 MPa and 8.65%, respectively, whereas the tensile strength and total elongation are 626 MPa and 24.37% in the soft regions, respectively [21]. To achieve the goal mentioned above, innovative processing techniques, such as selective heating, selective cooling, and selective tempering, are applied. The study showed that the material properties varied with tempering temperature and tempering time. Using this method, variable tensile strengths can be achieved from 700 to 1300 MPa in conjunction with elongation from 9.5% to 3% with the technique of localized tempering [22].

In order to meet the further demand for lightweight vehicle components, higher tensile strength steel has been developed. A new ultra-high-strength hot-rolled hot stamping steel alloyed with Cr and Si elements was developed by removing the chemical composition elements of B and Ti [23]. To enhance the surface quality and ensure the hardenability of hot stamping steel, an amount of Cr element was added. The excellent combination of high tensile strength of 2150 MPa and total elongation of 12% was reaped by adjusting the hot stamping process parameters. However, the most typical one is 38MnB5Nb ultra-high-strength hot stamping steel, of which the strength can be enhanced to as high as 2000 MPa after hot stamping or quenching treatment [24,25]. The change in the microstructure and mechanical properties of 38MnB5 steel through the addition of 0.054 Nb was investigated by Guo et al. [26]. The results indicated the microstructure is refined and the properties, including tensile strength, yield strength, as well as elongation, are enhanced with the addition of 0.054 Nb. In our previous work, the phase transformation behaviors of 38MnB5Nb ultra-high-strength hot stamping steel were discussed in detail with the help of CCT (continuous cooling transformation) curves with different cooling rates and TTT (time–temperature–transformation) curves with different isothermal temperatures [27]. It showed that compared with the conventional 22MnB5 ultra-high-strength hot stamping steel, the studied 38MnB5Nb ultra-high-strength hot stamping steel is more beneficial for selective cooling processes to obtain both soft regions and hard regions. To investigate the formability of 38MnB5Nb ultra-high-strength hot stamping steel, the flow behaviors at different high temperatures of it were deeply studied [28]. In addition, a complex model was established by taking the deformation temperature, the strain rate, and the types of microstructure into consideration. Finally, hot-stamped parts in the shape of a "U" were obtained and discussed by methods of numerical and experimental analysis. The study showed that the microstructure and hardness are varied with tempering processes, including tempering temperature and time [29]. Almost all parts should be tempered after quenching treatment. So, the tempering process plays a significant role in manufacturing parts, especially in terms of hot stamping steel components, such as a B-pillar. The study implied that the width of the transition zone of the component consisting of both soft regions and hard regions relies on the tailored tempering processes [30].

However, the study of hardness evolution during tempering for 38MnB5Nb ultra-high-strength hot stamping steel is rare. So, the references for designing tempering process parameters (temperature and time of tempering) are extremely few. At the same time, the hardness evolution of steel is critical for manufacturing high-quality components, especially

for manufacturing components that consist of both a soft region to absorb energy and a hard region to resist the intrusion mentioned above because of the application of the tempering processing during their manufacture. So, in this paper, the evolution behavior of hardness for 38MnB5Nb ultra-high-strength hot stamping steel during the tempering process after quenching is investigated through the method of modeling and an experimental method.

2. Methods

The normal chemical compositions of the investigated 38MnB5Nb ultra-high-strength hot stamping steels, which were manufactured through the process of hot rolling by Shou Gang Group in Beijing, China, are presented in Table 1. Compared with the conventional 22MnB5 hot stamping steels, a small amount of Nb is added, and the C content is increased slightly. It should be noted that both the addition of Nb and the increment of C content affect the microstructure transformation behavior during continuous cooling as well as the isothermal treatment and tempering process [26]. During the rolling stage, a part of the Nb is in the state of carbides, nitrides, or carbonitrides, which can refine grains, and the other part of the Nb is dissolved in the iron matrix to enhance the effect of the solid solution's strengthening [1]. On the other side, the precipitation during the tempering process of NbC is influenced by the addition of Nb and the increment of C content, which contribute to enhancing the strength (hardness) and the light weight of components, correspondingly. From our previous work, it can be known that the microstructure after hot rolling is composed of ferrite and pearlite [27]. From the result of the continuous cooling transformation (CCT) curve, it can be conjectured that the critical cooling rate is between 10 and 15 °C/s and that the austenite start temperature (A_{c1}) and austenite finish temperature (A_{c3}) are 748 °C and 805 °C, respectively [27].

Table 1. Compositions of the 38MnB5Nb steels (weight percentage, wt%).

Steel	C	Si	Mn	Cr	B	Nb	Fe
38MnB5Nb	0.36	0.24	1.39	0.19	0.005	0.05	Bal.

Before conducting the subsequent tempering experiments, preliminary heat treatments were performed on the 38MnB5Nb ultra-high-strength hot stamping steel plates. These plates had dimensions of 200 mm in length, 150 mm in width, and 2 mm in thickness. The heat treatments, as shown in Figure 1, included homogenization and quenching processes. The homogenization processes are as follows (Figure 1a): the plates were heated to 950 °C and held for 30 min, which was followed by cooling to the ambient temperature (approximately 30 °C) inside the furnace (Beijing Research Institute of Mechanical and Electrical Technology Ltd., Beijing, China). The quenching processes are as follows (Figure 1b): the aforementioned plates were heated to 920 °C and held for 5 min in the same furnace used for the homogenization processes, which was followed by water quenching to approximately 30 °C. The microstructure after quenching consists of martensite (Figure 2a,b) with a high density of dislocations (Figure 2c), as shown in Figure 2. The martensite is primarily lath martensite.

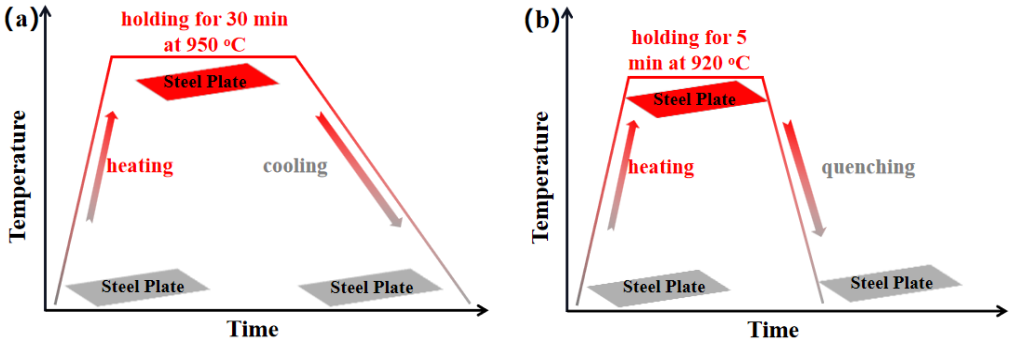


Figure 1. Schematic graphs of preliminary heat treatments: (**a**) homogenization processes; (**b**) quenching processes.

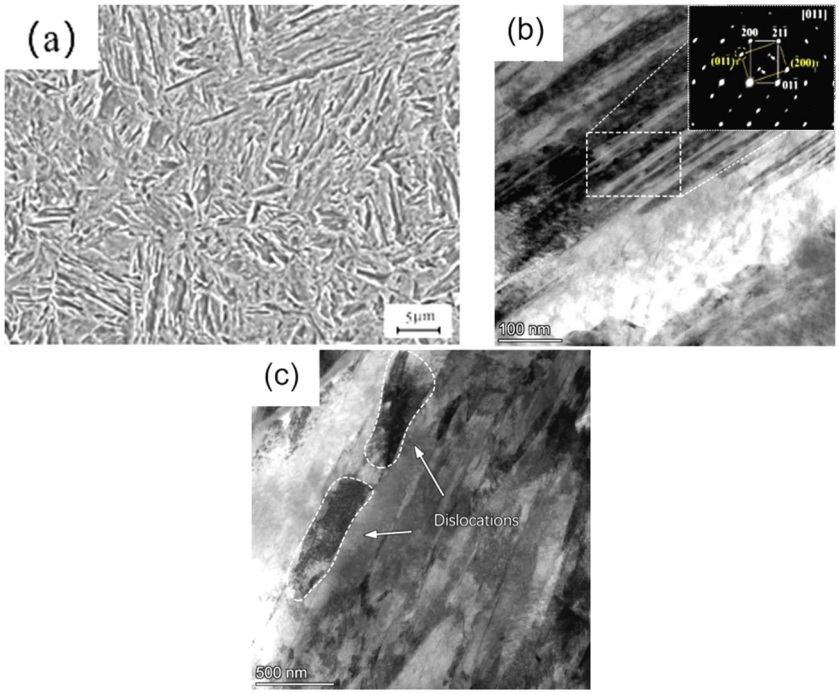


Figure 2. Microstructure after quenching of 38MnB5Nb steel: (**a**) SEM; (**b**) TEM for displaying phase; (**c**) TEM for displaying dislocation.

The tempering process experiments were carried out using a dilatometer (Bähr D805 L, Bachmuseum, Germany) equipped with quartz push-rods. During the dilatometer experiments, thermocouples were welded onto samples with sizes of 10 mm in length, 4 mm in width, and 2 mm in thickness. These samples were cut from steel plates using wire cutting after undergoing preliminary heat treatments, including homogenization treatment and quenching treatment. This was completed to ensure accurate temperature control throughout the entire tempering process in the dilatometer experiments. The tempering processes are as follows, as shown in Figure 3. Firstly, 48 samples were heated to 300 °C, 400 °C, 500 °C, 600 °C, 700 °C, and 800 °C with a heating rate of 40 °C/s, respectively; Secondly, the samples were held at the all above temperatures with the time of 10 s, 20 s, 50 s, 100 s, 200 s, 500 s, 1000 s, and 2000 s, respectively; Thirdly, the samples were rapidly cooled to 30 °C with cooling rate of 50 °C/s.

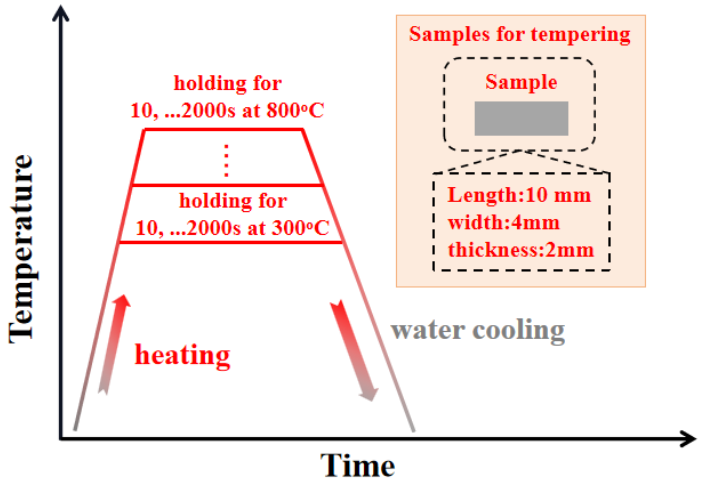


Figure 3. Schematic graph of the tempering processes for the samples with sizes of 10 mm in length, 4 mm in width, and 2 mm in thickness.

The following tempering experiments were conducted using samples with sizes of 150 mm in length, 50 mm in width, and 2 mm in thickness. The samples were placed into a tempering furnace (Beijing Research Institute of Mechanical and Electrical Technology Ltd., Beijing, China) at temperatures of 500 °C, 600 °C, and 700 °C and then held for approximately 40 s (as depicted in Figure 4), in sequence. Then, they were quickly removed from the furnace and cooled with water to approximately 30 °C. The above samples are named QT-500, QT-600, and QT-700, respectively. The samples that have just undergone preliminary heat treatments are named Q-30.

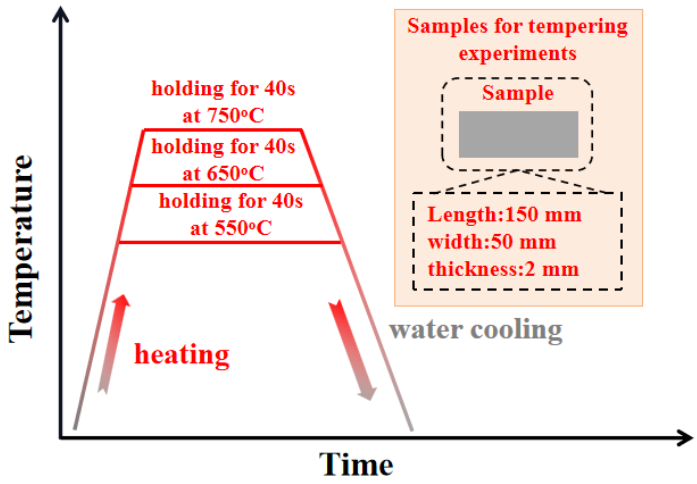


Figure 4. Schematic graph of tempering experiments for samples with sizes of 150 mm in length, 50 mm in width, and 2 mm in thickness.

The hardness of the samples treated with tempering processes was measured using an auto Vickers hardness tester (Beijing Times, Beijing, China). Meanwhile, the hardness of one sample that was not treated with tempering processes was also tested and found to have a value of 580 Hv, which stands for the hardness of the as-quenched state. The load was maintained at approximately 10 gf, and the time was kept for 10 s during the measurement of hardness. Notably, five values were obtained. The average value was adopted for all of the samples.

Scanning electronic microscopy (SEM, ZEISS EVO18, Oberkochen, Germany) was used to observe the microstructure of each specimen after polishing and etching in a 4% nital solution. Transmission electron microscopy (TEM, Talos F200X, Waltham, MA, USA)

was used to observe all possible morphologies of carbide. TEM observation was carried out on thin foils that were electropolished at −40 °C using a 4% perchloric acid solution.

A SUNS 5305 tensile tester (MTS Systems, Shenzhen, China) was applied to test the mechanical properties of standard tensile samples. The dimensions of the standard tensile samples are a gauge width of 5 mm, a gauge thickness of 2 mm, and a gauge length of 28 mm. Three samples were tested for each condition (including Q-30, QT-500, QT-600, and QT-700), and the average values were recorded.

3. Results and Discussions

3.1. The Hardness Evolution during Tempering

Generally, the microstructure of steels varies with changes in tempering processes, such as tempering temperature and tempering time [29]. Therefore, the hardness varies when the tempering processes vary. That is to say, the hardness is significantly affected by the parameters of tempering processes. Hardness evolution with time during tempering is shown in Figure 5a for the studied 38MnB5Nb ultra-high-strength hot stamping steel at different temperatures ranging from 300 to 700 °C. The results show that the hardness decreases as the tempering temperature rises under the same time condition. When the samples are tempered at 300 °C and 400 °C, the hardness is relatively high. When the samples are tempered at 600 °C and 700 °C, the hardness is relatively low. Moreover, the hardness value falls within the middle range for the samples tempered at 500 °C. The temperature range for high-temperature tempering of 38MnB5Nb hot stamping ultra-high strength steels is approximately 600 to 700 °C. The temperature range for low-temperature tempering of the studied steel is from 300 to 400 °C, while the remaining temperatures fall under middle-temperature tempering. Compared to other temperature ranges, the largest decrease occurs between 500 and 600 °C. Meanwhile, the hardness is decreased sharply during the initial stage of tempering at each temperature with a tempering time of 200 s. Then, a quasi-linear decrease in hardness takes place following the sharp decrease. Finally, the hardness decreased slightly with extended time; therefore, the hardness value remains relatively constant, depending on the tempering temperatures. It can be deduced that the same level of hardness can be achieved at different tempering temperatures by adjusting the tempering time. The change in hardness over time during isothermal treatment at 800 °C is also shown in Figure 5b. It can be seen that the hardness rapidly reduces to about 298 Hv and then increases to about 485 Hv. So, it can be deduced that the as-quenched martensite transforms into austenite when heated to 800 °C and held at that temperature. Subsequently, the austenite transforms back into martensite during the cooling stage. This is consistent with the results that the austenite start temperature (A_{c1}) and austenite finish temperature (A_{c3}) are 748 °C and 805 °C, respectively [27]. Obviously, heating the sample to 800 °C and holding it at 800 °C do not fall within the scope of tempering, because austenitization occurs. Thus, the following analysis does not include the process of heating to 800 °C and holding at that temperature.

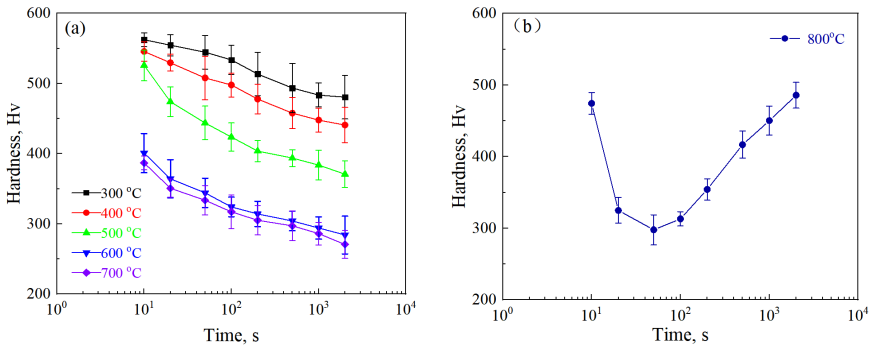


Figure 5. Hardness evolution with time during tempering at different temperatures ranging from 300 to 700 °C (**a**), and at a temperature of 800 °C (**b**).

3.2. The Construction of Tempering Model

Since hardness alone cannot accurately indicate the degree of softening from a quenched state to a quasi-equilibrium state, the tempering ratio is introduced. The softening degree is described by the following definition [30], which can be represented by Equation (1).

$$\tau = \frac{H_0 - H(t)}{H_0 - H_\infty} \quad (1)$$

where τ is the tempering ratio; H_0 is the hardness in the as-quenched state; H_∞ is the hardness in the annealed state, and $H(t)$ is the hardness after tempering at a specific temperature and time, whose value is between that of H_0 and that of H_∞. Obviously, according to this definition, tempering ratio values range from 0 (representing the as-quenched state) to 1 (representing the annealed state). For the studied 38MnB5Nb ultra-high-strength hot stamping steel, the experimentally measured hardness value of the sample that was tempered at 700 °C for 2000 s is regarded as H_∞, namely H_∞ = 274 Hv.

The evolution of the hardness ratio with time during tempering for different temperatures, ranging from 300 to 700 °C, is shown in Figure 6. The hardness ratio increases exponentially as the tempering time extends at the specified tempering temperature. The higher the temperature, the faster the hardness ratio increases during the initial period for the same tempering time. It is demonstrated that the tempering ratios increase when the tempering temperatures are raised while keeping the tempering time constant. This is because the hardness decreases as the temperature increases under the same tempering time condition.

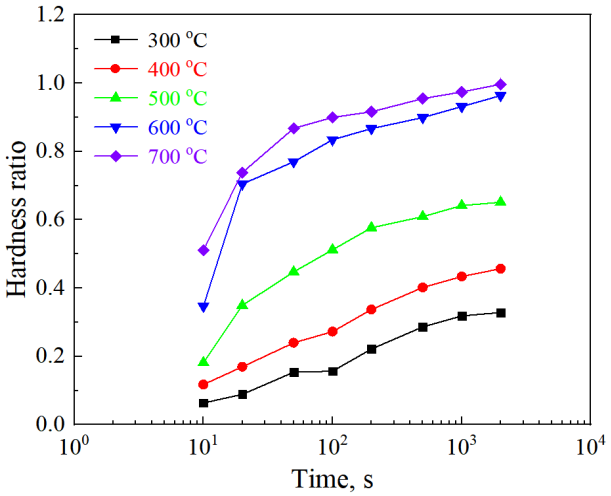


Figure 6. Evolution of hardness ratio with time during tempering for different temperatures between 300 and 700 °C.

Several models were proposed to describe the kinetics of tempering. It is well known that the evolution of the tempering ratio is controlled by the diffusion mechanism, as the precipitation and growth of carbides occur during tempering. In addition, carbides were formed relatively quickly during tempering in the 38MnB5Nb ultra-high-strength steel analyzed in Section 3.3 of this study. The tempering kinetic model, in the form of the Johnson–Mehl–Avrami-type equation, is applied to investigate the tempering kinetic [31]:

$$\tau = 1 - \exp(-Dt^n) \quad (2)$$

where t is the tempering time and n is the Avrami index determined by the material and preliminary treatments, such as casting, forging, and preliminary heat treatment. D is the

parameter affected by tempering temperature and can be described using the Arrhenius equation.

$$D = \mathrm{D_0}\exp\left(-\frac{\mathrm{Q}}{\mathrm{R}T}\right) \tag{3}$$

where $\mathrm{D_0}$ is the constant; Q is the activation energy of tempering temperature; R is the gas constant (8.31 $\mathrm{J}\times\mathrm{K}^{-1}\times\mathrm{mol}^{-1}$) and T is the absolute temperature. Generally, the value of $\mathrm{D_0}$ and Q varies from material to material.

Equations (4) and (5) are obtained by taking the natural logarithm of Equations (2) and (3), respectively.

$$\ln(\ln\frac{1}{1-\tau}) = \ln D + \mathrm{n}\ln t \tag{4}$$

$$\ln D = \ln \mathrm{D_0} - \frac{\mathrm{Q}}{\mathrm{R}T} \tag{5}$$

The relationship between $\ln(\ln\frac{1}{1-\tau})$ and $\ln t$ with different tempering temperatures is shown in Figure 7a. From Equation (4), it can be deduced that the value of the slope and intercept of each line in Figure 7a is equal to n and ln D, respectively, for the corresponding tempering temperatures. The values of n and ln D are obtained using the regression method, as shown in Table 2. The average value of n for the five lines in Figure 7a is selected: namely, the value of n in Equation (2) is 0.308.

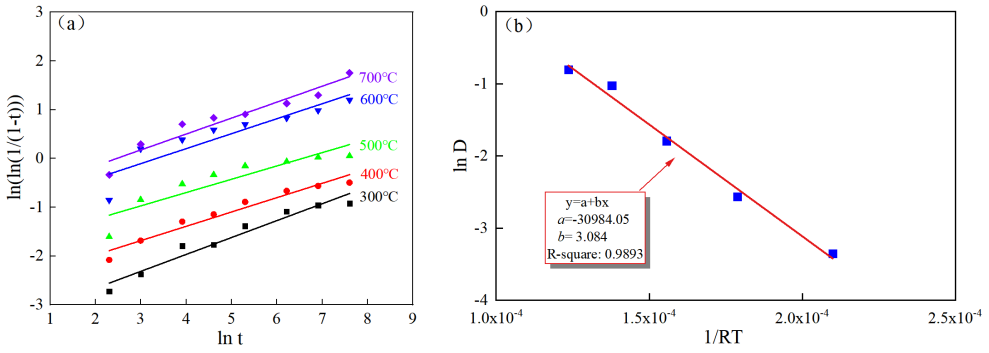


Figure 7. (**a**) Relationship between $\ln(\ln\frac{1}{1-\tau})$ and $\ln t$ with different tempering temperatures; (**b**) relationship between ln D and $\frac{1}{\mathrm{R}T}$ with different tempering temperatures.

Table 2. The values of n and ln D under different temperatures.

Parameters	Tempering Temperature, °C					Average
	300	400	500	600	700	
n	0.347	0.294	0.273	0.307	0.327	0.308
ln D	−0.805	−1.026	−1.790	−2.566	−3.355	-

The relationship between ln D and $\frac{1}{\mathrm{R}T}$ with different tempering temperatures is shown in Figure 7b. Similarly, the values of the slope and intercept of the line in Figure 7b are equal to −Q and $\ln \mathrm{D_0}$, respectively. So, the values of Q and $\ln \mathrm{D_0}$ are 30,984.05 and 3.084, respectively, that were obtained by the regression method. Then, the value of $\mathrm{D_0}$ is calculated, which is equal to 21.85. The Arrhenius equation can be expressed as follows:

$$D = 21.85\exp\left(-\frac{30984.05}{\mathrm{R}T}\right) \tag{6}$$

After obtaining these constants, the tempering kinetic model in the form of the Johnson–Mehl–Avrami type can be expressed by Equation (7).

$$\tau = 1 - \exp\left[-21.85\exp\left(-\frac{30984.04}{\mathrm{RT}}\right)t^{0.308}\right] \quad (7)$$

Combining Equations (1) and (2), the tempering hardness can be described by the following equation.

$$H(t) = \mathrm{H}_0 + (\mathrm{H}_\infty - \mathrm{H}_0)(1 - \exp(-\mathrm{D}t^{\mathrm{n}})) \quad (8)$$

So, the hardness after tempering of the studied 38MnB5Nb ultra-high-strength hot stamping steel can be predicted using Equation (9) for a given tempering temperature and time.

$$H(t) = 274 + 316\left\{1 - \exp\left[-21.85\exp\left(-\frac{30984.04}{\mathrm{RT}}\right)t^{0.308}\right]\right\} \quad (9)$$

The experimental results and calculated hardness for the studied 38MnB5Nb ultra-high strength steel are presented in Figure 8. It shows that the experimental results fit very well with the calculated results, which, in turn, demonstrates that the constructed tempering model in this study can accurately describe the evolution of hardness during tempering.

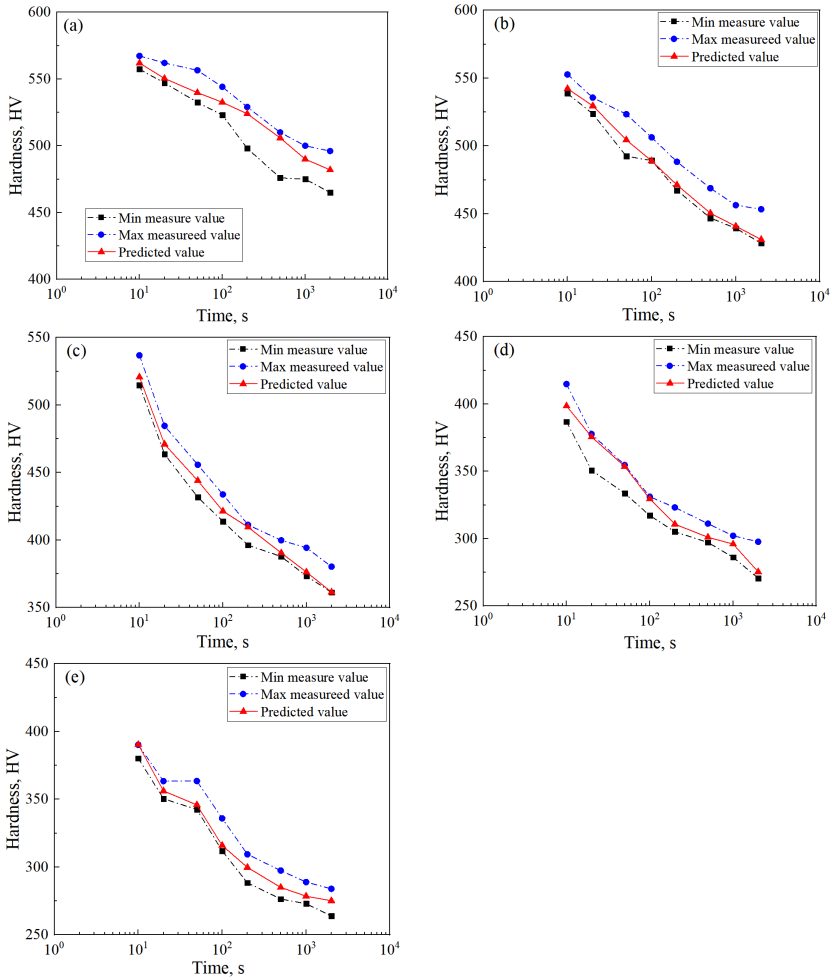


Figure 8. Comparison between the experimental and predicted hardness of the 38MnB5Nb steels after undergoing various tempering processes: (**a**) tempering at 300 °C; (**b**) tempering at 400 °C; (**c**) tempering at 500 °C; (**d**) tempering at 600 °C; (**e**) tempering at 700 °C.

3.3. Application of the Tempering Model

The hardness values of samples with dimensions of 150 mm in length, 50 mm in width, and 2 mm in thickness, which were subjected to different tempering temperatures of 500 °C, 600 °C, and 700 °C for approximately 40 s, are 378.5 ± 15, 325.4 ± 12, and 286.1 ± 17, respectively, as depicted in Figure 9. The values calculated with Equation (9) are also displayed in Figure 9. It can be observed that the calculated values align well with the measured values, indicating that the developed tempering model for 38MnB5Nb ultra-high-strength hot stamping steel is capable of predicting the hardness of the steel after tempering treatment at various tempering temperatures and durations.

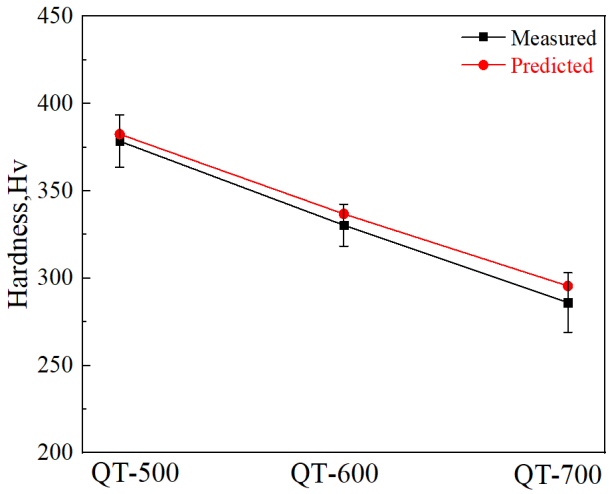


Figure 9. The comparison between measured hardness and predicted hardness.

The SEM microstructure of each sample is shown in Figure 10 after being tempered at different temperatures for the same amount of time. Compared to the as-quenched state, the microstructure becomes unclear after tempering treatment, particularly the lath interface, and martensite undergoes decomposition. Martensitic laths merge during tempering, and as the tempering temperature increases, the degree of merging also increases. When the tempering temperature increases to 700 °C, the characteristic of the lath disappears. As shown in Figure 10d,e, the TEM images indicate the precipitation of numerous carbides. The changes in hardness after tempering heavily depend on the microstructure. The relationship between the tempering processes, the microstructure, and the change in hardness is consistent with the reference results.

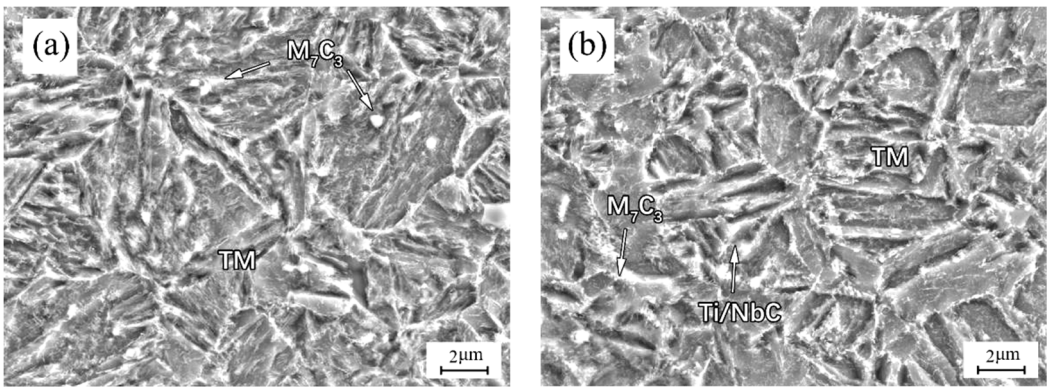


Figure 10. *Cont.*

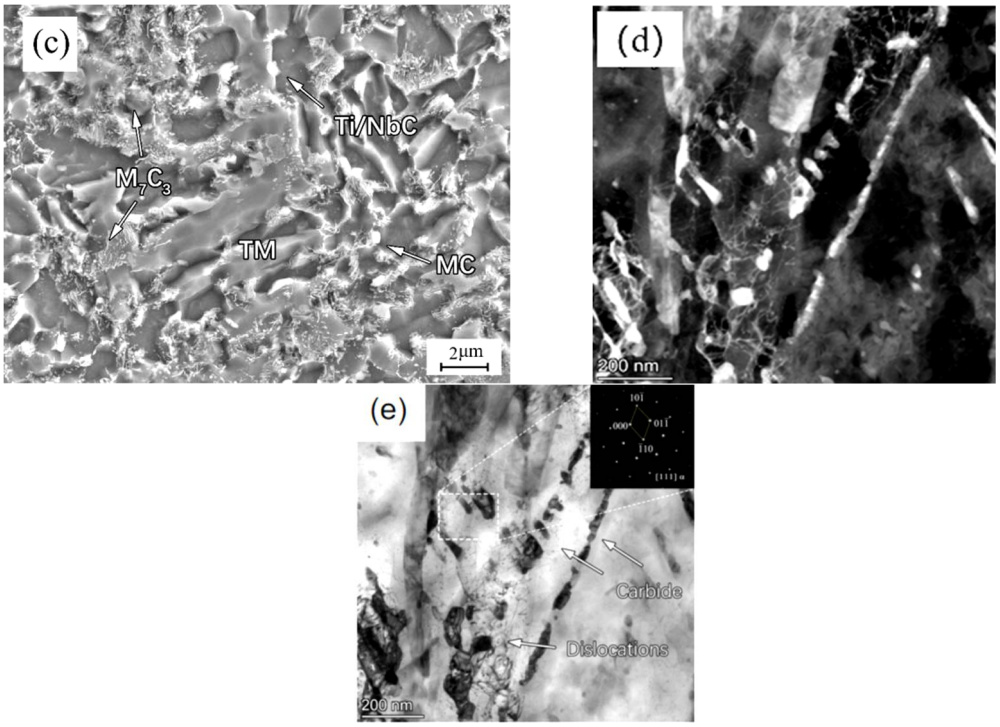


Figure 10. SEM microstructure of the samples with the tempering time of 40 s and different temperatures: (**a**) 500 °C; (**b**) 600 °C; (**c**) 700 °C; (**d**) TEM microstructure of the samples with tempering time of 40 s and temperature of 700 °C; (**e**) TEM dark field microstructure of the samples with tempering time of 40 s and temperature of 700 °C.

The mechanical properties of the Q-30, QT-500, QT-600, and QT-700 samples are listed in Table 3. Each value in Table 3 represents the average obtained from three tests under the same conditions. The tempering process has a significant impact on mechanical properties, indicating that the mechanical properties can be customized by adjusting tempering process parameters. For example, compared to the Q-30 samples, the samples tempered at 500 °C, 600 °C, and 700 °C for 40 s exhibit lower strength and improved ductility. The product of strength and elongation (PSE) obtained for the Q-30, QT-500, QT-600, and QT-700 samples is higher than that of the Q-30 samples, which is beneficial for improving the ability to absorb crash energy. With the increase in tempering temperature, the strength (including tensile strength and yield strength) decreases. This phenomenon is consistent with the tendency that hardness decreases as the tempering temperature increases.

Table 3. Mechanical properties of the samples.

Samples	Rm (MPa)	Rp0.2 (MPa)	TEL (%)	PSE (GPa%)
Q-30	1986	1476	6.8	13.5
QT-500	1252	880	15.8	19.8
QT-600	1116	772	16.8	18.7
QT-700	987	642	18.8	18.6

Rm, tensile strength; Rp0.2, yield strength; TEL, total elongation; PSE, product of strength and elongation.

4. Conclusions

The evolution of hardness during tempering for 38MnB5Nb ultra-high-strength hot stamping steel is analyzed using experimental and modeling methods. An accurate tem-

pering model was developed to predict the hardness after tempering using various tempering processes, such as tempering temperature and time. The following conclusions are summarized.

The hardness of the 38MnB5Nb ultra-high-strength steel is significantly influenced by tempering process parameters, such as tempering temperature and time. The hardness decreased as the tempering temperature increased under the same time condition.

The hardness of the 38MnB5Nb ultra-high-strength steel in the quenched state is about 580 Hv, while it is 240 Hv in the quasi-annealed state.

As the tempering time extends, the hardness decreases sharply in the initial stage. Then, it decreases in a quasi-linear trend with a slight slope. Finally, the hardness reaches an almost constant value, which depends on the tempering temperature.

Compared to the Q-30 sample, the samples after tempering exhibit lower strength and improved ductility. The product of strength and elongation (PSE) obtained for the Q-30, QT-500, QT-600, and QT-700 samples is higher than that of the Q-30 samples.

Based on the hardness of the quenched state, tempered state, quasi-annealed state, tempering ratio, and tempering kinetic law, an accurate tempering model is established to describe the evolution of hardness with temperature and time during the tempering process of the 38MnB5Nb ultra-high-strength hot stamping steel.

Author Contributions: Conceptualization, P.L. and Z.T.; Methodology, P.L. and X.L. (Xianjun Li); Software, M.Z.; Validation, Z.T. and X.L. (Xiao Liang); Formal analysis, P.L. and J.L.; Investigation, P.L.; Resources, X.L. (Xianjun Li) and W.Z.; Data curation, M.Z., K.W., P.H., J.L. and X.L. (Xiao Liang); Writing—original draft, P.L.; Writing—review and editing, X.L. (Xianjun Li), W.Z. and Z.T.; Visualization, M.Z., K.W., P.H. and X.L. (Xiao Liang); Supervision, W.Z. and J.L.; Funding acquisition, X.L. (Xianjun Li). All authors have read and agreed to the published version of the manuscript.

Funding: This research was funded by the Ministry of Industry and Information Technology High-Quality Development Special Project of China, grant number 202223222302, and the National Science and Technology Major Project of China, grant number 2018ZX04023002.

Data Availability Statement: Not applicable.

Acknowledgments: The authors express thanks to the Ministry of Industry and Information Technology High-Quality Development Special Project of China, grant number 202223222302, and the National Science and Technology Major Project of China, grant number 2018ZX04023002. Special thanks to Decheng Wang and Chao Jiang for their guidance and supervision.

Conflicts of Interest: The authors declare no conflict of interest.

References

1. Chen, H.; Zhao, L.; Lu, S.; Lin, Z.; Wen, T.; Chen, Z. Progress and Perspective of Ultra-High-Strength Martensitic Steels for Automobile. *Metals* **2022**, *12*, 2184. [CrossRef]
2. Zhang, W.; Xu, J. Advanced Lightweight Materials for Automobiles: A review. *Mater. Des.* **2022**, *221*, 110994. [CrossRef]
3. Zhang, Y.; Lai, X.; Zhu, P.; Wang, W. Lightweight Design of Automobile Component using High Strength Steel Based on Dent Resistance. *Mater. Des.* **2006**, *27*, 64–68. [CrossRef]
4. Romain, P.; David, L.; Eric, P. Use of Multi-scale Approach for Vehicle Weight Reduction Study. *Procedia Eng.* **2023**, *66*, 403–414.
5. Huang, W.; Gu, H.; Liu, Q.; Si, T. Suppression of Hydrogen-induced Damage in 22MnB5 Hot Stamping Steel by Microalloying. *Mater. Chem. Phys.* **2020**, *256*, 123729. [CrossRef]
6. Zhang, J.; Ji, L.; Bao, D.; Feng, Y.; Li, S.; Weng, Y. Gigacycle Fatigue Behavior of 1800 MPa Grade High Strength Spring Steel for Automobile Lightweight. *J. Iron Steel Res. Int.* **2014**, *21*, 614–618. [CrossRef]
7. Masoud, A.; Amy, B.; Jimi, T.; Chandra, V.; Omar, F.; Mohini, S. Prediction of Greenhouse Gas Emissions Reductions Via Machine Learning Algorithms: Toward an Artificial Intelligence-based Life Cycle Assessment for Automotive Lightweighting. *Sustain. Mater. Technol.* **2022**, *31*, e00370.
8. Gupta, M.; Singhal, V. Review on Materials for Making Lightweight Vehicles. *Mater. Today Proc.* **2022**, *56*, 868–872. [CrossRef]
9. Hultgren, g.; Boåsen, M.; Narström, T.; Barsoum, Z. Fracture Toughness Assessment of Surface Cracks in Slender Ultra-high-strength Steel Plates. *Eng. Fract. Mech.* **2023**, *289*, 109458. [CrossRef]
10. Li, K.; Yang, T.; Gong, N.; Wu, J.; Wu, X.; Zhang, D.; Murr, L. Additive Manufacturing of Ultra-high Strength Steels: A Review. *J. Alloys Compd.* **2023**, *965*, 171390. [CrossRef]

11. Song, C.; Zhang, Z.; Wu, W.; Wang, H.; Sun, Z.; Yang, Y.; He, W.; Xu, J.; Xia, Y.; Yin, W.; et al. Effect of Si on the Dislocation Date within Martensite of Ultra-high Strength Hot-rolled Medium Mn Steel with Good Ductility. *Mater. Sci. Eng. A* **2023**, *869*, 144825. [CrossRef]
12. Quan, G.; Zhan, Z.; Zhang, L.; Wu, D.; Luo, G.; Xia, Y. A Study on the Multi-phase Transformation Kinetics of Ultra-high-strength Steel and Application in Thermal-Mechanical-Phase Coupling Simulation of Hot Stamping Process. *Mater. Sci. Eng. A* **2016**, *673*, 24–338. [CrossRef]
13. Mor, K.; Okuda, Y. Tailor Die Quenching in Hot Stamping for Producing Ultra-high strength Steel Formed Parts Having Strength Distribution. *CIRP Ann.* **2010**, *59*, 291–294. [CrossRef]
14. Liu, S.; Long, M.; Zhang, S.; Zhao, Y.; Zhao, J.; Feng, Y.; Chen, D.; Ma, M. Study on the Prediction of Tensile Strength and Phase Transition for Ultra-high Strength Hot Stamping Steel. *J. Mater. Res. Technol.* **2020**, *9*, 14244–14253. [CrossRef]
15. Liang, J.; Lu, H.; Zhang, L.; Li, F.; Gao, R.; Liu, K.; Pan, H.; Teng, H.; Li, X.; Guo, A.; et al. A 2000 MPa Grade Nb Bearing Hot Stamping Steel with Ultra-high Yield Strength. *Mater. Sci. Eng. A* **2020**, *9*, 14244–14253. [CrossRef]
16. Thawin, H.; Johannes, B.; Alexander, H.; Markus, B.; Marion, M. A Unified Model for Isothermal and Non-isothermal Phase Transformation in Hot Stamping of 22MnB5 Steel. *J. Mater. Process. Technol.* **2023**, *313*, 117856.
17. Çavuşoğlu, O.; Çavuşoğlu, O.; Yılmazoğlu, A.; Üzel, U.; Güral, A. Microstructural Features and Mechanical Properties of 22MnB5 Hot Stamping Steel in Different Heat Treatment Conditions. *J. Mater. Res. Technol.* **2020**, *9*, 10901–10908. [CrossRef]
18. Min, J.; Lin, J.; Min, Y. Effect of Thermo-mechanical Process on the Microstructure and Secondary-deformation Behavior of 22MnB5 Steels. *J. Mater. Process. Technol.* **2013**, *213*, 818–825. [CrossRef]
19. Berglund, D. Hot Stamped Components with Tailored Properties-Simulation and Validation of Product Performance. *Steel Grips* **2010**, *8*, 41–44.
20. Cantergiani, E.; Fillon, A.; Lawrence, B.; Sauvage, X.; Perez, M.; Scott, C.; Weck, A. Tailoring the mechanical properties of steel sheets using FeC films and diffusion annealing. *Mater. Sci. Eng. A* **2016**, *657*, 291–2298. [CrossRef]
21. Tang, B.; Li, Q.; Wang, Q.; Guo, N.; Meng, X.; Shi, Y.; Su, H.; Lin, L. A Novel Micromechanical-Based Secant Method to Predict the Elastoplastic Constitutive Relation of a Tailor-tempered 22MnB5 Sheet. *Mater. Today Commun.* **2022**, *31*, 103236. [CrossRef]
22. Bao, L.; Wang, B.; You, X.; Li, H.; Gu, Y.; Liu, W. Numerical and Experimental Research on Localized Induction Heating Process for Hot Stamping Steel Sheets. *Int. J. Heat Mass Transf.* **2020**, *151*, 119422. [CrossRef]
23. Zhao, Y.; Yang, D.; Qin, Z.; Chu, X.; Liu, J.; Zhao, Z. A Novel Hot Stamping Steel with Superior Mechanical Properties and Antioxidant Properties. *J. Mater. Res. Technol.* **2022**, *21*, 1944–1959. [CrossRef]
24. Song, R.; Pottore, N.S. Martensitic Steels with 1700–2200 MPa Tensile Strength. Patent EP2785888B1, 8 October 2014.
25. Jo, M.C.; Yoo, J.; Kim, S.; Kim, S.; Oh, J.; Bian, J.; Sohn, S.S.; Lee, S. Effects of Nb and Mo alloying on resistance to hydrogen embrittlement in 1.9 GPa-grade hot-stamping steels. *Mater. Sci. Eng. A* **2020**, *789*, 139656. [CrossRef]
26. Lin, L.; Li, B.; Zhu, G.M.; Kang, Y.-L.; Liu, R.-D. Effects of Nb on the Microstructure and Mechanical Properties of 38MnB5 Steel. *Int. J. Miner. Metall. Mater.* **2018**, *25*, 1181–1190. [CrossRef]
27. Luo, P.; Li, X.; Zhang, W.; Liang, X.; Tan, Z.; Wang, D.; Jiang, C.; Hou, J.; Sun, L. The Study of Phase Transformation Behaviors for 38MnB5Nb Ultra High-Strength Steel by CCT Curves and TTT Curves. *Metals* **2023**, *13*, 190. [CrossRef]
28. Liang, X.; Li, X.; Wang, D.; Lin, X.; Luo, P.; Tan, Z.; Song, Y.; Tian, Y.; Hou, J.; Jiang, C.; et al. Numerical and Experimental Study on Hot Forming by Partition Cooling of 38MnB5Nb. *Metals* **2022**, *12*, 839. [CrossRef]
29. Shi, L.; Ran, X.; Zhai, Y.; Pan, Y.; Zhang, S.; Cheng, X.; Tang, B.; Wang, H. Influence of Isothermal Tempering on Microstructures and Hydrogen-environmentally Embrittlement Susceptibility of Laser Additively Manufactured Ultra-high Strength AerMet100 Steel. *Mater. Sci. Eng. A* **2023**, *876*, 145167. [CrossRef]
30. Zhang, Z.; Delagnes, D.; Bernhart, G. Microstructure Evolution of Hot-work Tool Steels During Tempering and Definition of a Kinetic Law Based on Hardness Measurements. *Mater. Sci. Eng. A* **2004**, *380*, 222–230. [CrossRef]
31. Johnson, W.; Mehl, R. Reaction Kinetics in Processes of Nucleation and Growth. *Trans. Am. Inst. Min. Metall. Eng.* **1939**, *135*, 416–442.

Disclaimer/Publisher's Note: The statements, opinions and data contained in all publications are solely those of the individual author(s) and contributor(s) and not of MDPI and/or the editor(s). MDPI and/or the editor(s) disclaim responsibility for any injury to people or property resulting from any ideas, methods, instructions or products referred to in the content.